

Phenomenological forecasting of disease incidence using heteroskedastic Gaussian processes: a dengue case study

Leah R. Johnson* Robert B. Gramacy† Jeremy Cohen‡
 Erin Mordecai§ Courtney Murdock¶ Jason Rohr|| Sadie J. Ryan**
 Anna M. Stewart-Ibarra†† Daniel Weikel††

Abstract

In 2015 the US federal government sponsored a dengue forecasting competition using historical case data from Iquitos, Peru and San Juan, Puerto Rico. Competitors were evaluated on several aspects of out-of-sample forecasts including the *targets* of peak week, peak incidence during that week, and total season incidence across each of several seasons. Our team was one of the winners of that competition, outperforming all other teams in multiple targets/locals. In this paper we report on our methodology, a large component of which, surprisingly, ignores the known biology of epidemics at large—in particular relationships between dengue transmission and environmental factors—and instead relies on flexible nonparametric nonlinear Gaussian process (GP) regression fits that “memorize” the trajectories of past seasons, and then “match” the dynamics of the unfolding season to past ones in real-time. Our phenomenological approach has advantages in situations where disease dynamics are less well understood, or where measurements and forecasts of ancillary covariates like precipitation are unavailable and/or where the strength of association with cases are as yet unknown. In particular, we show that the GP approach generally outperforms a more classical generalized linear (autoregressive) model (GLM) that we developed to utilize abundant covariate information. We illustrate variations of our method(s) on the two benchmark locales alongside a full summary of results submitted by other contest competitors.

Key words: epidemiology, Gaussian process, heteroskedastic modeling, latent variable, generalized linear (autoregressive) model, dengue fever

*Corresponding author: Department of Statistics, Virginia Tech, Hutcheson Hall, 250 Drillfield Drive Blacksburg, VA 24061, USA ; 1rjohn@vt.edu

†Department of Statistics, Virginia Tech

‡Department of Integrative Biology, University of South Florida

§Department of Biology, Stanford University

¶Department of Infectious Diseases and Odum School of Ecology, University of Georgia

||Department of Integrative Biology, University of South Florida

**Department of Geography, University of Florida

††Department of Medicine, SUNY Upstate Medical University

‡‡Department of Biostatistics, University of Michigan

1 Introduction

According to the United States Centers for Disease Control and Prevention (CDC) more than one-third of the world’s population lives at risk of infection from dengue, a viral disease transmitted by *Aedes aegypti* and *Aedes albopictus* mosquitos. In the tropics and sub-tropics dengue is one of the leading causes of mortality and morbidity among viral vector-borne diseases (<http://www.cdc.gov/Dengue>, December 2016). Although the first dengue vaccine was licensed in Mexico in December 2015, the World Health Organization (WHO) recommends it only be used in geographic areas with high disease burden (World Health Organization, 2016), and it is not available throughout most of Latin America. As a result, prevention measures focus on avoiding mosquito bites and controlling mosquito populations. Although initial infections are often mild, subsequent infections can be very serious, leading to potentially life threatening disease manifestations, such as hemorrhage, shock, and death (World Health Organization, 2009).

Early recognition and prompt treatment of severe cases can substantially lower the risk of medical complications and death. Accurate forecasts of cases of infected individuals, or *incidence*, are key to planning and resource allocation. For example, knowing well in advance the numbers of cases that are expected and when they will occur allows preparation via education and community mobilization campaigns, reallocation of resources (people, insecticide, diagnostic reagents) to high-risk areas, or re-training of physicians to recognize symptoms and to treat appropriately (Kuhn et al., 2005; Degallier et al., 2010; Thomson et al., 2008) in advance of peak transmission.

In 2015 several agencies of the US federal government (Department of Health and Human Services, Department of Defense, Department of Commerce, and the Department of Homeland Security) joined together, with the support of the Pandemic Prediction and Forecasting Science and Technology Interagency Working Group under the National Science and Technology Council, to design an infectious disease forecasting project with the aim of galvanizing efforts to predict epidemics of dengue. Details of this “Dengue Forecasting Project” are available on the web pages of the National Oceanic and Atmospheric Administration (<http://dengueforecasting.noaa.gov/>), and will be summarized in Section 2. The basic idea is to allow competitors to train on historical incidence data, independently at two sites (Iquitos, Peru and San Juan, Puerto Rico), and then make forecasts for the full remainder of an epidemic season as weekly incidence numbers arrive. Competitors are judged relative to one another via proper scoring rules on several predictive *targets*, including peak incidence, peak week, and total season incidence (described in more detail below).

Our team was one of six top performing teams selected to present our methods to the White House Office of Science and Technology Policy and the Federal Pandemic Prediction and Forecasting Science and Technology Working Group at an event at the White House in October 2015. Our method was consistently among the best of competitors in all three targets, although not for absolutely all weeks of every season, as we will illustrate in Section 5. Surprisingly, a substantial component of our strategy deliberately ignores known associations between incidence and environmental variables such as precipitation and temperature. Instead we preferred a more phenomenological approach that modeled relationships in the

incidence data *only*, and developed a dynamic forecasting tool that attempted to determine, as the season unfolded, which of previous seasons the current one most resembles. The tools included data transformations, Gaussian processes, heteroskedastic components, latent variables, and Monte Carlo sampling of forecasted incidence trajectories. Below we refer to this as the **hetGP** (for heteroskedastic Gaussian Process) approach.

Our use of GPs toward this end is novel, although others have used GPs in epidemiological forecasting exercises in slightly different contexts. For example Farah et al. (2014) use GPs to emulate an SIR-type computer model in a forecasting framework for influenza, and Hu and Ludkovski (2015) deploy GPs within stochastic control framework involving a continuous time Markov process inspired by SIR models. Our **hetGP** predictor relies novel extensions to the typical GP arsenal: a multitude of variance components which are learned from data to achieve the heteroskedastic effect, and a latent variable scheme that allows forecasts to adapt to emerging season dynamics. Both of these terms, *heteroskedastic* (e.g., Binois et al., 2016) and *latent variable* (e.g., Bornn et al., 2012) can be found attached to GP methodology in the literature. However again our treatment of those, with choices motivated by our application to disease forecasting are, we believe, both new.

Our team also developed, in parallel, a forecasting apparatus based on a more conventional dynamic generalized linear model (GLM) framework, utilizing lagged environmental (e.g., precipitation and temperature) and demographic (e.g., population) covariates. The GLM occasionally out-performed **hetGP**. Since we could only submit one comparator to the contest, we opted for a hybrid of the two as a hedge. In this paper we focus our exposition on **hetGP**. We showcase its forecasting prowess in isolation, as compared to the GLM alone, to our original hybridized model, and to the results reported by other contest competitors. Besides un-coupling **hetGP** from the GLM, the **hetGP** version presented here is slightly updated from our contest submission. The original **hetGP** worked with a different data transformation, and deployed a more crude heteroskedastic mechanism. In our exposition we are careful to delineate the original contest submission and its more recent update, and to motivate the enhancements subsequently made.

The remainder of the paper is outlined as follows. In Section 2 we review contest particulars, with details on the transmission of dengue and its relationship to environmental covariates. We also introduce the data, discuss appropriate transformations, and summarize the contest scoring metrics that impacted some of our methodological choices. Section 3 provides a description of our main modeling contribution, **hetGP**. Section 4 discusses implementation details, including a classical GLM strategy. In Section 5 we provide visualization of our learning and forecasting procedures over the contest seasons, and a full comparison of our results against those of other contest entrants. We conclude with a brief discussion in Section 6. A lengthy appendix contains supplementary views into the data, an exploration of transformations, and technical details including analytic derivative expressions for the **hetGP** likelihood, a list of the environmental and demographic predictors that were key to the GLM setup, and an influential derived predictor based on a parameterized model of the so-called *basic reproductive rate*, R_0 .

2 Dengue forecasting project

Below we summarize the competition setup described in more detail on NOAA's website:

http://dengueforecasting.noaa.gov/docs/project_description.pdf

The “Dengue Forecasting Project” was announced in the first half of 2015, with training data up to 2009 made publicly available in June. For San Juan, Puerto Rico, the data go back to 1990, and for Iquitos, Peru, back to 2000. Competitors “registered” for the competition by submitting a brief report and results on the training data, treating the latter four years (2005-2009) as an out-of-sample testing set. Those successfully submitting initial results were invited to participate in the real testing exercise, which comprised of data from 2009-2013. Only invited teams received these data, delivered later in August, and with the understanding that it could not be shared with other parties. Forecasts on the testing data were due one week later, in early September. The quick turnaround meant that methods must be reasonably computationally efficient to be competitive.

2.1 The data

The provided data include weekly dengue incidence and linked environmental variables, and the training and testing sets may be downloaded from predict.phiresearchlab.org/legacy/dengue/index.html. The dengue incidence portion is comprised of historical surveillance data at Iquitos, Peru and San Juan, Puerto Rico, summarized weekly. Cases in the data set include laboratory-confirmed and serotype-specific cases. The data are actual final counts, i.e., reflecting the total number of cases in each week, possibly revised or estimated *ex post*. A breakdown of incidence into strata of four serotypes, with a fifth un-serotyped category, were also provided. However, we only trained on **total_cases** in the data file, i.e., the same variable that we were tasked with predicting out of sample.

As an example of the data, in Figure 1 we show San Juan incidence over the first sixteen years of the training period. Observe that there is a yearly cycle, although the severity and timing from one year to the next does not suggest an obvious pattern. Occasionally there are two bumps in a season. Notice that the data clearly exhibit a heteroskedastic feature, i.e., in addition to having a mean response that changes over time, the dispersion of points around that mean response also varies. This is most easily seen by comparing the 1991/1992 season to the 2000/2001 season, with the former having much larger spread than the latter. Visually, dispersion is correlated with level: the larger the levels the larger the dispersion. Naturally, the dispersion is also asymmetric due to positivity.

Sometimes such level-dependent variability and asymmetry can be simultaneously mitigated with a log transformation. Indeed, our originally submitted solution involved GP modeling on log (one-plus) incidence. However the log transformation over-corrects: lower dispersions are too spaced out relative to larger ones, which are aggressively squashed (see Figure A1). A square-root transformation works much better. Since forecasts based on Gaussians may be negative, the inverse transformation cannot involve squaring. Therefore

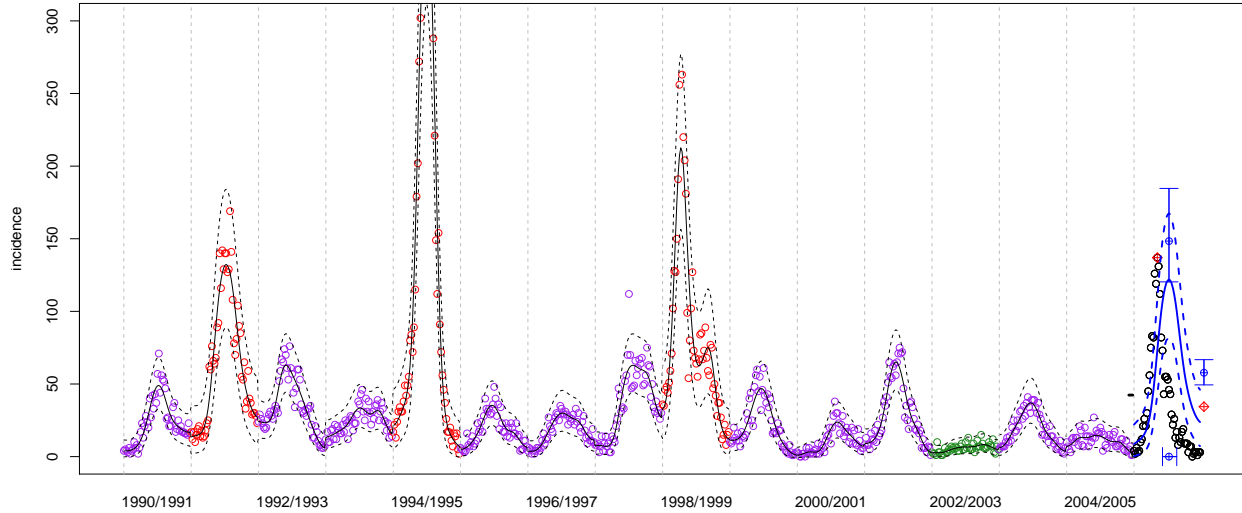


Figure 1: San Juan incidence data (open circles) over most of the training period. Incidence here are the number of reported cases of dengue each week. The colors indicate a judgment of severity in data that have been observed, specifically: green = mild (< 25 cases in any week), purple=moderate (25-100 in any week), red = severe (> 100 cases in any week). Future, unobserved data are indicated with black open circles. Solid lines indicate the posterior mean predictive surface and dashed lines the 90% quantiles around this mean. The black lines are the with-sample fits. The blue lines are the forecasted dynamics for the unobserved season. In the unobserved season, red circles indicate the true values of targets, blue open circles indicate point estimates for the targets and predictive intervals around those are indicated with blue error bars.

our revised method utilizes a continuous hybrid between the square root and log so that the inverse exponentiates negative forecasts. [For details, see Appendix A.1].

The contest organizers also provided environmental and demographic data as potential covariates, as it is widely known that environmental factors impact the dynamics of mosquito vectors and thus transmission dynamics (e.g., Moore et al., 1978; Johansson et al., 2009; Barrera et al., 2011; Lambrechts et al., 2011; Stewart-Ibarra et al., 2013; Xu et al., 2016). The data provided included weekly precipitation, temperatures (min, max, and average), habitat indices (specifically the normalized difference vegetation index (NDVI) a measure of presence of live green vegetation), and yearly population. Participants were free to augment with other social media, environmental and demographic covariates, but were barred from using dengue incidence measures from other (e.g., nearby) locations. Previous studies have identified correlations between the Southern Oscillation Index (SOI) and other El Niño sea surface temperature indices and dengue (e.g., Gagnon et al., 2001; Johansson et al., 2009). Our team obtained current monthly SOI and sea surface temperatures (Reynolds et al., 2002) and aligned these with the weekly case data to augment our data set.

An exploratory analysis revealed strong correlations between (lagged values) of these predictors and the `total_cases` response. For example, the correlations to average temperature and average squared temperature peak at around eleven weeks in the in-sample, training portion of our data, and these exhibit the highest linear correlation amongst the covariates provided. Other previous studies indicate similar long lags between environmental

covariates and incidence measures for dengue (Johansson et al., 2009; Stewart-Ibarra and Lowe, 2013; Stewart-Ibarra et al., 2013; Xu et al., 2016).

2.2 Forecasts and evaluation

Three predetermined forecasting targets are evaluated: peak week, peak incidence, and total incidence, revised every four weeks in each 52-week “season”. These are evaluated separately at the two sites, Iquitos and San Juan, for six targets total. Peak week referrs to a forecast of the week having the highest incidence, and peak incidence is the count of the number of (newly) infected individuals in that week. Total or season incidence refers to the sum of weekly incidences over all 52 weeks. Contest organizers asked for point estimates for each target, together with a predictive distribution discretized into “buckets” for each of thirteen weeks evenly spanning the season (i.e., one forecast every 4 weeks, starting from week zero). Competition evaluation focused on logarithmic scores over the first 24 weeks of each season in the testing set. These log scores are a variation on Example 3 from Gneiting and Raftery (2007): an aggregate of the natural logarithm of the probability p_i where i is the “bucket” containing true value of each target/week. The “bucket” discretization(s) and other details are provided in the contest rules document. Log scores are intended to evaluate forecasts based on a coherent blend of their accuracy and confidence.

As an example of forecasts for the three targets, refer again to Figure 1 for San Juan. The final season segment, delineated by the vertical dashed-gray bars, corresponds to (as yet unobserved) incidence in the 2005/2006 season shown as black open circles. The blue solid and dashed lines in that segment are a forecast of the incidence trajectory using only data from previous seasons, via the `hetGP` method described in Section 3. There are two open red circles with red crosses through them indicating the true values of the three targets. The y -coordinate of the first open red crossed circle indicates peak incidence, and the x coordinate indicates peak week. The y -value of the second open red crossed circle, drawn at the position of week “53” shows total incidence (divided by 52 so that it is on the same scale as the weekly incidence values). These are the targets for the current season, but they are unknown to the fitting and prediction method in the out-of-sample forecasting exercise(s). Predictions for these targets are shown as blue open circles with blue ‘I’-shaped error bars through them, representing 95% confidence intervals. There are three of these, one each for peak incidence, peak week (on the x -axis), and total incidence (at the position of week 53). We describe how these point forecasts and intervals, and ultimately the full predictive distribution over these targets, are derived in Section 4.2.

It is worth remarking that our modeling efforts do not explicitly leverage the form of the targets or the log score evaluation. We simply model historical incidence and derive predictions for future incidence. However our distributions for the targets, which are derived from the predictive distribution, are designed to be coherent with the evaluation scheme.

3 Gaussian process modeling

Our team’s initial approach to modeling the dengue challenge data was via the GLM described in Section 4.1; however there were several shortcomings. We found that parameters for environmental predictors lacked stability when trained on fewer than seven years of data (particularly problematic for Iquitos) and early season forecasts consistently under-estimated the potential for large epidemics. We were unable to address these weaknesses with linear models despite entertaining many diverse incarnations. Moreover, obtaining accurate forecasts for environmental predictors such as weekly precipitation was particularly fraught. Note that this is necessary even when using, say, lag-11 predictors if forecasting the full remaining season’s trajectory, up to 52 weeks into the future. Precipitation and SOI modeling, for example, were ultimately deemed to be harder than the original incidence modeling problem as accurate forecasting almost certainly requires climate models.

Thus we decided to explore a second approach based on Gaussian processes (GPs). This alternative strategy is simultaneously simpler (in its use of data) and far more flexible (non-parametrically estimating non-linear relationships). In fact it uses no observed covariates other than the (square-root transformed) series of weekly incidence numbers, and therefore no environmental or other predictors required forecasting subroutines.

The basic idea behind the GP was to build a fitting mechanism that “memorized” the incidence trajectories of previous seasons, in a certain statistical sense, and thus could produce forecasts for the current season that resemble previous, similar seasons. At the start of a season, before any new data have arrived, we desired forecasts based almost entirely on an amalgam of previous seasons, with an adjustment for starting level (taken from the end of the previous season) and a conservative “hedge” involving severity, biasing forecasts towards more extreme past seasons while awaiting data which hopefully suggest the contrary. Then, as the forecasting season progresses, we desired a fitting mechanism which could be updated quickly (in light of the new data), so that predictions could be tailored to track some previous seasons more closely than others, but be flexible enough to exhibit/track novel behavior depending on what the incoming data suggested. The details follow.

3.1 A simple GP fit on derived variables

Gaussian process (GP) regression is an established nonparametric modeling apparatus originating in the spatial statistics literature, where it is also known as *kriging* (Matheron, 1963; Cressie, 1993). The GP has recently gained popularity in the machine learning literature (Rasmussen and Williams, 2006). For our purposes a GP is simply a flexible model $y(x) = f(x) + \varepsilon$, facilitating nonparametric regression given example training pairs (y_i, x_i) . When choosing predictors x_i it helps to think spatially, rather than linearly as with more standard regressions (like GLMs). That is, the GP will give more similar predictions (i.e., more highly correlated) for $y(x)$ and $y(x')$ if x and x' are close in the input space. Following a common default in the GP prediction literature, we measure that correlation as a product

of exponential inverse squared distances in the coordinates of x via

$$C_\theta(x, x') = \exp \left\{ - \sum_{k=1}^p \frac{(x_k - x'_k)^2}{\theta_k} \right\}, \quad (1)$$

a so-called product (or separable) Gaussian kernel. The characteristic *length-scale* hyperparameter θ_k in each input coordinate k , or weight on distances in each x_k , can be learned from the data through the likelihood. The unknown quantities are referred to as hyperparameters, rather than ordinary parameters, due to the nonparametric nature of GP prediction and to the subtle effect their settings have on those predictions. Default values are often sufficient to get highly accurate results. We briefly digress to review some relevant specifics GPs before continuing with details on how we deploy GPs for dengue incidence forecasting.

3.1.1 GP review

The model for a finite collection of $Y(x)$ -variables, $Y_n = (y_1, \dots, y_n)$ observed at a row-wise collected matrix of inputs $X_n = [x_1^\top; \dots; x_n^\top]$ in GP regression is multivariate normal (MVN), which is where the term Gaussian process comes from.¹ A typical setup is

$$Y_n \sim \mathcal{N}_n(m(X_n), \tau^2(C_n + \eta \mathbb{I}_n)) \quad (2)$$

where $C_n \equiv C_\theta(X_n, X_n)$ is an $n \times n$ matrix constructed from $C_\theta(x_i, x_j)$ pairs of rows of X_n . The scale parameter τ^2 and the so-called *nugget* η may be estimated along with θ by reinterpreting (2) as a likelihood. Appendix B provides an expression for the log likelihood, a *concentrated* version with closed form maximum likelihood estimator (MLE) for the scale $\hat{\tau}^2$ plugged in, and one for the gradient of the concentrated log likelihood comprised of partial derivatives with respect to all parameters. That discussion is tailored to our heteroskedastic (**hetGP**) extensions described shortly in Section 3.3, but comments therein also address the simpler case described here. Observe that the ordinary linear model is nested within the GP framework as a special case if we take $m(X_n) = \beta[1; X_n]$ and $C(\cdot, \cdot) = 0$ and $\eta = 1$. Many GP modeling setups take $m(\cdot) = 0$ unless one has *a priori* knowledge of mean dynamics. This has the effect of moving all of the modeling effort to the correlation structure.

The forecasting distribution then arises as a consequence of MVN conditioning rules. Let \mathcal{X} denote a set of predictive locations. The GP setup extends the MVN to the joint distribution of data $Y_n \equiv Y(X_n)$ and n' predictive $\mathcal{Y} \equiv Y(\mathcal{X})$ quantities. Using $m(\cdot) = 0$ and dropping θ from $C_\theta(\cdot, \cdot)$ to streamline the notation,

$$\begin{bmatrix} \mathcal{Y} \\ Y_n \end{bmatrix} \sim \mathcal{N}_{n'+n} \left(0, \begin{bmatrix} C(\mathcal{X}, \mathcal{X}) + \eta \mathbb{I}_{n'} & C(\mathcal{X}, X_n) \\ C(X_n, \mathcal{X}) & C(X_n, X_n) + \eta \mathbb{I}_n \end{bmatrix} \right).$$

The conditional distribution is $\mathcal{Y} | Y_n, X_n, \mathcal{X}, \theta, \eta, \tau^2 \sim \mathcal{N}_{n'}(\mu(\mathcal{X}), \Sigma(\mathcal{X}))$ where

$$\begin{aligned} \text{mean} \quad \mu(\mathcal{X}) &= C(\mathcal{X}, X_n)(C_n + \eta \mathbb{I}_n)^{-1} Y_n \\ \text{and variance} \quad \Sigma(\mathcal{X}) &= \tau^2(C(\mathcal{X}, \mathcal{X}) + \eta \mathbb{I}_{n'} - C(\mathcal{X}, X_n)(C_n + \eta \mathbb{I}_n)^{-1} C(X_n, \mathcal{X})). \end{aligned} \quad (3)$$

¹I.e., not from the choice of kernel with a Gaussian form; a GP can involve any kernel function that induces a positive semi-definite correlation structure.

With most choices of covariance kernel note that $C(\mathcal{X}, \mathcal{X}) = 1$. Inference (via MLE, say) and prediction (following the equations above) is fairly straightforward to code, however many libraries exist. Our contest submission implementation used the `newGPsep`, `jmleGPsep`, and `predGPsep` functions in the `laGP` library (Gramacy, 2014, 2016) for R (R Development Core Team, 2008) on the Comprehensive R Archive Network (CRAN). Those functions serve as the basis for extensions provided by our new `hetGP` library, implementing the new (revised) methods we describe shortly in Section 3.3.

3.1.2 GP dengue incidence forecasting

To use this setup to forecast dengue incidence requires “divining” some x -variables to pair with the square-root-transformed y incidence values. We say “divining” because a unique, and perhaps at first somewhat puzzling, feature of our approach is that (unlike the GLM in Section 4.1) we deliberately avoid environmental and demographic predictors known to covary with dengue incidence. Our x -values are entirely determined by fixed values we create in order to encourage the dynamics we observe in the training data, and by the dengue incidence (y) values themselves. Nevertheless, through inference for hyperparameters, particularly the θ s, the GP predictors we calculate are able to accurately track trajectories as they evolve in time by learning the appropriate “spatial” length-scale, which acts as a similarity measure between y -values depending on the close-ness of their associated x ’s.

We use the four predictors described below.

- x_1 : Season–time. Our first predictor is the repeated sequence $1, \dots, 52$, corresponding to the week number of the response y -value. This causes the response y -values to be modeled as more highly correlated with one another if they come from the same or nearby weeks in the current season *and* other seasons.
- x_2 : Starting level. Our second predictor is the value of the final y -value in the previous season. This x_2 -value is repeated for each of the 52 observations in each season, and encodes our belief that the season-dynamics are more similar (more highly correlated) to other seasons which started at similar levels. For the first season in each data set we take the first value of the season instead.
- x_3 : Sine wave. Our third predictor acknowledges periodic effects, for example, as may be driven by temperature and precipitation, but more importantly encodes that the end of all seasons should be correlated with their beginnings and the beginnings of others, and vice-versa. Like x_1 this is a deterministic predictor that is repeated for all seasons.
- x_4 : Severity. Based on the y -values (on the original scale) this predictor takes on one of three values $\{-1, 0, 1\}$ depending on the value of the largest number of cases in a week during that season. For example, for the San Juan incidence data, if there are more than 100 cases in any week in a particular season, then the x_4 value for all observations in that season is set to 1, recording a severe season. If no week has more than 25 cases it is set to -1 , a mild season. Otherwise it is set to zero, indicating an intermediate

level. The open circles in Figure 1 are colored by this x_4 value: -1 is green, 0 is purple, and red is $+1$. For Iquitos the thresholds are 25 and 10 , respectively. Therefore, x_4 encodes that the dynamics of severe seasons should be more similar to one another than to intermediate or (to a lesser extent) mild ones.

Clearly x_4 is unknown as a particular season unfolds, during which time forecasts are being derived from predictive distributions. It is a so-called *latent variable* in this context, requiring special treatment as we describe below. Its settings, $\{-1, 0, 1\}$ are arbitrary and its relationship to the y -values is deliberately weak. In other settings, perhaps a higher dimensional variable with a stronger link to y may work as well or better. Our rather simple setup is preferred primarily for its implementation advantages; i.e., it is the simplest setup we could envision that provided the requisite flexibility.

3.2 Forecasting, latent learning, and nonstationary dynamics

At the start of a new forecasting season, i.e., at week zero, all historical observations are used to form the x and y -values that comprise the training set. Maximum likelihood is used to infer the unknown hyperparameters. Forming a predictor for the following weeks involves assembling the x -values describing those weeks, and then running them through the predictive equations as \mathcal{X} values (3). In the case of x_1, x_2, x_3 this is straightforward; x_4 is more challenging because the severity of the new season is an unknown quantity. (Part way through the season we may know if the maximum incidence is above 100 say, but if it is not the chances that it will be are a complicated function of the evolving dynamics and noise in the data.) To address this we treat the new-season x_4 value as a *latent variable* whose setting is initially set conservatively to indicate a moderately severe season. In our contest submission that was accomplished with an initial setting of $x_4 = 0.5$. The details of our revised version are provided in Section 3.3. As data arrive throughout the season we use the so-called *predictive log likelihood* to optimize its setting.

Our use of the predictive log likelihood involves the model's predictive probability of observed data y'_1, \dots, y'_j from the first j weeks of the new season, paired with inputs $x'_i = (x'_{i1}, x'_{i2}, x'_{i3}, x'_{i4})$, for $i = 1, \dots, j$. This is calculated following Eq. (3), evaluating the (log) MVN density with y' as \mathcal{Y} and the x' as \mathcal{X} . To choose latents we view that log predictive probability as a function of x'_{i4} , which in our setup is the same for all i , and optimize over that value. That is, if S represents a set of severity values of interest, then one solves

$$\hat{x}'_{.4} = \operatorname{argmax}_{x_{.4} \in S} p(y' | x', Y_n, X_n, \dots) \quad (4)$$

to obtain an estimate of the latent severity coordinate $\hat{x}'_{.4}$. In Equation (4) the \dots refer to settings of the GP hyperparameters, e.g., MLE settings. Especially early in the season we find it helpful to restrict S to a small window (e.g., ± 0.25) around the previous $\hat{x}'_{.4}$ estimated from earlier weeks in the season, starting with $\hat{x}_{.4} = 0.5$ at week zero.

As an illustration, consider the week-zero season forecasts corresponding to the setup in Figure 1. We re-draw a zoomed-in version of the figure here, in the left panel of Figure 2. With a latent structure indicating moderate-to-high severity, and a low setting of the

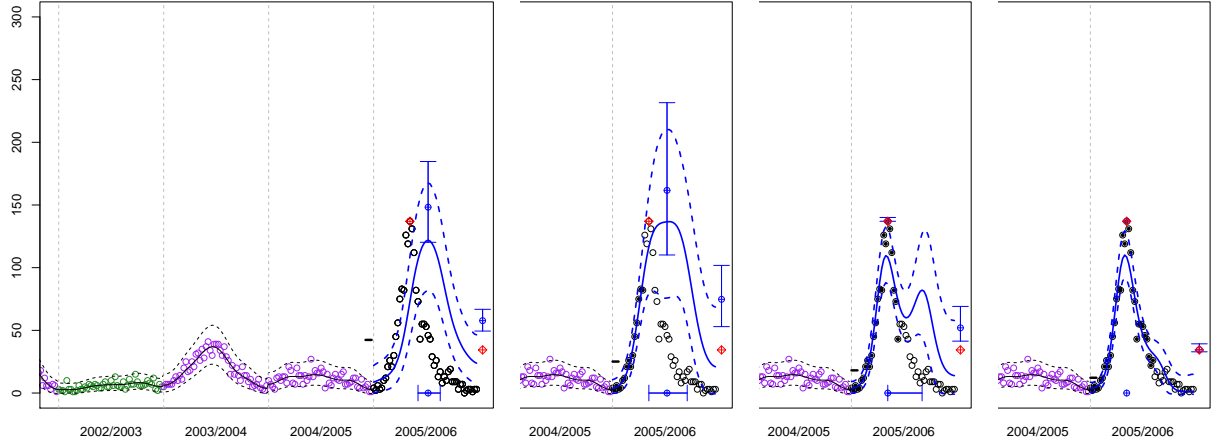


Figure 2: Snapshots of GP forecasts for San Juan corresponding to weeks 0, 16, 24 and 32 in the 2005/2006 season. Symbols, colors, and plotting lines are the same as in Figure 1.

starting level x_2 , we can see [referring to Figure 1] that the week-zero forecasts most resemble the mildest of the severe historical seasons (1991/1992). However the other seasons, both milder and more extreme, contribute to the forecasts via the exponentially decaying distances calculated in the GP covariance structure.

As the season progresses the model fit learns that it is indeed a severe year. The second panel of Figure 2 shows the revised predictive equations after data up to week 16 are incorporated. (Incorporated weeks have their open circles filled in with solid dots.) Observed incidences are on an upward trend, and we can see from the future data that the peak is yet to come. It is perhaps not surprising then that the forecasts of potential future incidence, and the associated uncertainty, have increased substantially compared to week zero. However, eight weeks later, shown in the third panel, the observed incidences are declining, and the forecasts indicate that it is quite likely that the peak has passed. The probabilities associated with that hypothesis, and the associated error-bars shown in the figure, are explained in Section 4.2. Observe that the forecasting distribution indicates the potential for a relapse of high incidence, mimicking the observed dynamics of 1998/1999. After another eight weeks, shown in the final panel, the potential for such a relapse is much diminished.

Towards the end of the season it is typical for the estimated latent \hat{x}_4 value to drift away from $\{-1, 0, 1\}$ values that encode the fourth coordinate of the training data X_n . This is because each season is distinct from the previous ones, and capturing those distinct dynamics requires the new season to exhibit differences rather than similarities to the past. Moreover, it is clear from examining Figure 1, or the transformed versions in Figure A1, that the dynamics are highly nonstationary. However, our Gaussian correlation structure assumes stationarity (i.e., that the correlation depends only on distance between the inputs). In particular, observe that within-season dynamics do not have the same mean structure from one season to the next, and therefore exhibit a degree of nonstationarity. The introduction of a latent coordinate has recently been proposed as a remedy for adapting a stationary GP to nonstationary data (Bornn et al., 2012). Therefore there is a tension in the dual role

we are asking $x_{.4}$ to take on: indicating severity (i.e., similarly to certain past seasons with similar incidence heights) and nonstationary flexibility (i.e., dissimilarity to any previous year, whether by height or otherwise).

3.3 Heteroskedastic enhancements

During the contest period we noticed a relationship between seasonal severity (i.e., mean weekly incidence) and the dispersion of incidences around their mean. That is, we noticed that the data were heteroskedastic, even after using the square root (and log) transformations [Appendix A.1] in an attempt to minimize such relationships. However due to time constraints imposed by the contest deadlines we were unable to develop the methodological extensions required address this nuance for our original submitted forecasts. Figure 3

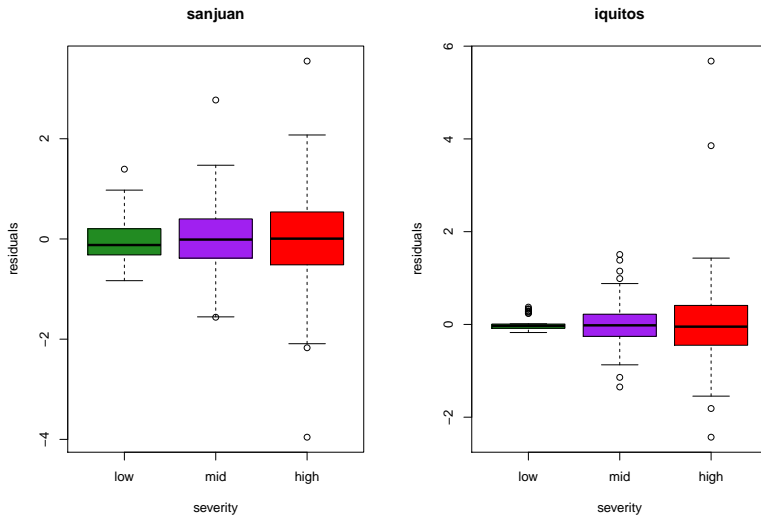


Figure 3: Residual errors from the homoskedastic GP fit to the square root transformed data by severity level for San Juan (left) and Iquitos (right) training data.

illustrates this feature of the data by plotting in-sample residuals from the weekly predicted mean fitted values obtained over the training period for San Juan and Iquitos. These results are on the scale of the square-root transformed y -values. Observe that residuals for seasons classified as low severity (less than 25 weekly cases for San Juan and less than 10 for Iquitos) show the lowest dispersion, whereas residuals for the highest severity seasons (more than 100 and 25, respectively) show the highest dispersion. Therefore, even after using the x_4 variable to account for dynamics differentiated by seasonal severity, there is potentially un-accounted for variation in uncertainty that could adversely effect our forecasting distributions and the log scores that were used to judge contest participants.

To address this issue in our revised method we introduced an indicator variable based on x_4 , the severity input, to modulate the nugget η in our covariance function (2), allowing it to differentiate by seasonal severity. In particular, we re-define the MVN covariance as

$\tau^2(C_n + \Lambda_n)$ where Λ_n is a diagonal matrix with entries

$$\lambda_i = \begin{cases} \eta_{-1} & x_{i4} = -1 \\ \eta_0 & x_{i4} = 0 \\ \eta_{+1} & x_{i4} = +1. \end{cases} \quad (5)$$

The newly created three-vector hyperparameter $\eta = (\eta_{-1}, \eta_0, \eta_{+1})$ may be inferred by MLE via extensions to the closed form derivative calculations on the log likelihood, as we detail in Appendix B. We observe very little difference in the computational demands required to infer the three-vector η parameter compared to its scalar, i.e., homoskedastic, counterpart in (2). There is nothing special about having three categories; should a practitioner believe there are more or less than three severities, for instance, the calculations are the same. Indeed, Appendix B's presentation is engineered so that, e.g., the scalar version clearly arises as a special case. However a different approach may be desired for cases where severity is likely to smoothly vary with the other inputs. In that case, *stochastic Kriging* (SK, Ankenman et al., 2010) may present an attractive alternative. However, note that SK requires replication of observations to obtain stable input-dependent variance estimates. That could only be accomplished in our setup by restricting x_2 , the starting level input, to a small discrete set of values, which (in experiments not detailed herein) has deleterious effects.

The final ingredient in our `hetGP` scheme is to extend the latent learning strategy of Section 3.2 to the noise level utilized for new season forecasts. With only three, discrete, choices $\{\eta_{-1}, \eta_0, \eta_{+1}\}$ it is straightforward to evaluate the MVN predictive log likelihoods under each choice by assigning all λ_i in the new season alternately to each η -value. Then rather than picking one, we weight the three sets of resulting forecasts according to those predictive probabilities within the Monte Carlo scheme outlined in Section 4.2.

4 GLM comparator and implementation details

Below we outline a somewhat more standard generalized linear model (GLM)-based comparator. We focus here on a high-level description, emphasizing a particularly useful derived predictor based on the basic reproductive rate, R_0 , relegating details on other (lagged) predictors to Appendix C.1. We conclude the section with a description of a Monte Carlo framework for generating forecasts for both GP and GLM-based comparators, and a brief commentary on how we produce the particular summaries required for contest submission.

4.1 A GLM approach

Our preferred GLM models the `total_cases` response using a negative binomial family with a log link and with computation facilitated by `glm.nb` in the `MASS` library (Venables and Ripley, 2002) for R. Our predictors include a deterministic time index (to allow for a temporal trend), auto-regressive components, population size, environmental variables, and deterministic sine/cosine functions to capture broad seasonal effects. In addition to these covariates we included a scaled version of the basic reproductive number of the epidemic, R_0 ,

as a function of temperature. This measure was derived and parameterized using previously published data on how mosquito traits depend on temperature, following methods developed in Mordecai et al. (2013) and Johnson et al. (2015). Brief details are provided in Appendix C.2 and full details for the particular case of dengue are presented by Mordecai et al. (2017).

Most of the (non-deterministic) predictors were smoothed using a one-sided filter with equal weights over the preceding 10 weeks (via `filter` in R). Some of the covariates entertained were cumulatively derived (e.g., by summing up precipitation over the weeks preceding forecasts) in a particular season. To initialize a suitable set of potential covariates, and in particular to identify suitable transformations and lags and to find appropriate phases for the deterministic trigonometric predictors, we performed an extensive exploratory analysis on the training data (up through the 2004/2005 season).

In each out-of-sample forecasting week we re-train the GLM. The first step involves selecting variables amongst the universe of deterministic, derived, accumulated lagged and transformed predictors via Bayes Information Criterion (BIC), which is automated by `step` in R. Forecasts are then derived from the selected model. Forecasts beyond one week ahead that condition on predictors, like temperature, will necessitate forecasting subroutines. Separate Gaussian time-series models are fit for these predictors. The full historical data are used, up to the current forecasting week, but otherwise these sub-models are far simpler in flavor compared to the original `total_cases` GLM, and favor autoregressive, trend, and trigonometric components. Note that these sub-models are needed even when the `total_cases` GLM uses substantially lagged predictors. For example, a lag 11 predictor requires full forward propagation to be utilized twelve or more weeks into the future.

Finally, a Monte Carlo scheme, described in more detail in Section 4.2, is used to propagate uncertainty in sub-modeled predictors through to forecasts of `total_cases` in subsequent weeks. Compounding errors in the autoregressive sub-model forecasts can obliterate the influence of those predictors, especially for end-of-season forecasts made early in the season. This “washing out” was one of the substantial drawbacks of the GLM approach that motivated our `hetGP` alternative. An example of such forecasts, mirroring Figure 2, is shown in Figure 4. Although the historical data are colored in green, as open circles, the color does not indicate severity, as unlike in the `hetGP` setup, there is no such (latent) indicator variable in the GLM. The predictive curves are more “jagged” owing to a higher Monte Carlo error arising from additional forward simulation of predictors. Observe the overly optimistic forecasts early in the season (first) panel. The `hetGP` method is much better at “matching” to previous similar seasons before the current season’s dynamics begin to unfold. Later in the season the GP and GLM are more comparable, although a notable exception in this example is the lack of a (potential) second hump in the third panel compared to Figure 4.

4.2 Monte Carlo for forecast targets

We deployed a Monte Carlo (MC) post-processing scheme to obtain point estimates and distributions for the contest targets: peak incidence, peak week, and season incidence. In the case of the GP predictor this involved sampling from the MVN predictive equations (3). For the GLM it meant sampling first from sub-modeled predictors (e.g., via `predict.lm`

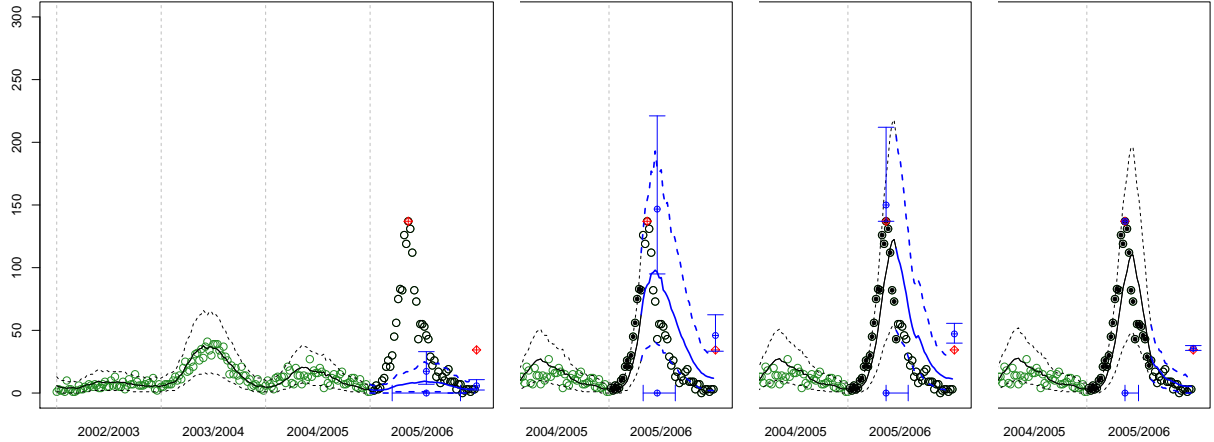


Figure 4: Snapshots of GLM forecasts for San Juan. Here the colors, lines, and symbols are the same as in Figures 1 and 2, except that we do not include the severity indicator and instead the green open circles correspond to data from historical seasons.

in R), and then conditionally from the negative binomial GLM using the associated `predict` method. Samples from the three targets may then be obtained via simple identification rules. For instance, the distributions of peak week and peak incidence are determined by the frequency of MC samples indicating that a particular week has the highest sampled incidence values, and the incident value at the highest week, respectively. Season incidence is simply the sum over those weekly samples.

After sample trajectories are converted into target samples, their distribution can be summarized in a variety of ways (e.g., by histogram); we show them as intervals in Figure 2, on which we offer further comment shortly. Point estimates can be derived by extracting the most frequent week, the average highest observed weekly incidence, and the average sum over the weeks, respectively. In our new multiple-nugget `hetGP` version [Section 3.3], the nugget for the forecasting season is sampled in the MC scheme according to the weights calculated from the predictive log likelihood of the forecasting season data so far observed. Our original contest submission involved a hedge that acknowledged some of the GLM limitations alluded to previously. We used MC to hybridize (non-heteroskedastic) GP and GLM by ignoring GLM sampled forecasts obtained from fewer than seven years of historical data, and those based only first three four-weekly forecasts, taking GP ones only for those forecasting weeks. Otherwise, MC samples from both methods were combined equally.

Although both GP and GLM setups *can* provide a full sample over all weeks in the season, regardless of the forecasting week (even for past weeks), the contest rules made it inefficient to regard “backcasts” as random variables. That is, if the observed peak incidence so far is in week ten, then for all weeks before or after week ten any observed incidence below the week-ten incidence *should* be regarded as having zero probability of being a peak week or having peak incidence, irrespective of model predictions. Although we believe this would be the wrong way to present target forecasts in a real-world setting, we adjusted our MC scheme to replace simulated values by observed values up to the forecasting week in order

to maximize our contest score.

An example of the effect of this can be seen in the third panel of Figure 2. Observe that the peak week interval is truncated on the left by the point estimate because the MC samples have been post-processed so that historical times cannot take on any other value than what was actually observed. Although the interval “contains” other observed weeks that had values less than the historical peak (red dot), this is an artifact of our display of the peak week target as a connected interval. The set of weeks with a positive probability of being a peak week may be disconnected—especially later in the season. As can be seen in the third panel, only one or two weeks in the second “hump” of the forecasting distribution have a chance of besting the historical peak week observed so far in that season.

Before turning to an exhaustive analysis of our empirical results, we make a final remark here about computational demands. Model fitting is relatively fast; it is the MC forecasting scheme that is computationally expensive. GP fitting and prediction, although typically requiring flops that are cubic in the data size, n , takes seconds (for each forecasting week) with a well designed C implementation linking to accelerated linear algebra libraries (e.g., Intel MKL) on the data sizes we entertain (e.g., $n = 520$ for ten years of historical data). GLM fitting, even with `step` searches, is similarly speedy. Including sub-model fits for predictors, this approach requires tens of seconds for obtaining fits and forecasts. However, obtaining enough MC samples to make smooth forecasting plots (Figures 2 and 4) and thus deduce accurate target distributions, requires millions of draws from predictive distributions. For the MVNs behind `hetGP` (3), this is still reasonably fast because a joint sample over all season–weeks can be taken at once, requiring tens of seconds for the largest n . In contrast, GLM forecasting with the nested sub-model predictions is much slower because propagation must proceed step-by-step, in a Markov fashion, over the weeks of the season. The result is a scheme that requires several minutes for each forecasting week.

5 Empirical results

Below we summarize our out-of-sample results on the contest data in two views. First is an “absolute” view, illustrating our forecasts on their own merits against the six *true* targets. The second is a “relative” view, comparing our results to those of other contest entrants.

5.1 Absolute view

In lieu of a full suite of four-weekly panels as in Figures 5–6, requiring 208 panels across locations and training and testing phases (separately for each comparator, `hetGP` and GLM), we instead provide a more compact summary in terms of point estimates and intervals.² While intervals offer a convenient visualization, note that actual predictive uncertainty sets may be disconnected. The presentation here focuses on our `hetGP` results.

Figure 5 shows the four-weekly results for San Juan. The partition into training and testing sets corresponds to the phases of the contest, not to the nature of the data: all

²Our suppliment provides a slide-show-like rendition akin to Figures 5–6 for the interested reader.

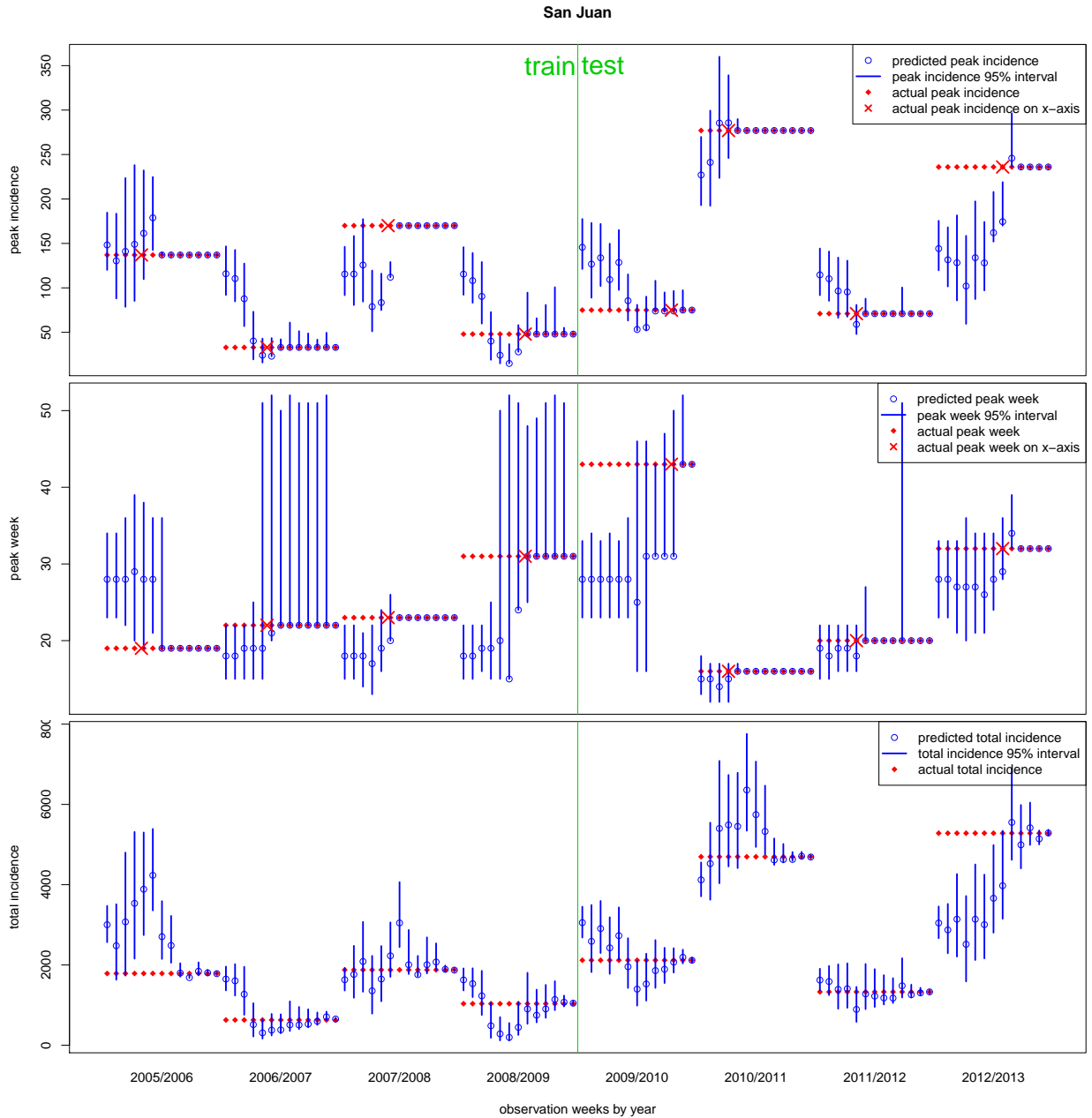


Figure 5: Weekly progress of out-of-sample forecasts at San Juan, separated by the training and testing period. Top: peak incidence; Middle: peak week; Bottom: total incidence. The forecasts are in blue, showing points (open circles) and intervals. The true targets are solid diamonds in red, shown on both x (week) and y (target) as appropriate.

forecasts are out-of-sample. Notice our early season forecasts for San Juan are by no means perfect. We typically, but not always, capture the peak week and peak incidence (top two panels) within our 95% interval several weeks before the actual observed peak week (red \times). Once the observed peak week arrives, our intervals quickly shrink to point masses around the true values. That is, we have very little backcasting error, an exception perhaps

being 2011/2012 for all three targets. Our peak week predictions are nearly always in the ballpark—an exception perhaps being 2009/2010 peak week, whose true peak occurs much later than that of any previous season. We have a tendency to over-shoot early forecasts in mild seasons, owing to our pessimistic initialization of the latent variable. A notable exception is the 2012/2013 season. This one is particularly hard to predict because, as we show in the *left* panel of Figure A2 of Appendix A.2, it represents an extrapolation. There is no historical data “nearby”, either in the data space (i.e., historical peak incidence or peak week), or in the predictor space (say in terms of starting level, x_2). Therefore we underforecast peak incidence, and thus total incidence, early in that season.

Figure 6 summarizes our results in the much more challenging Iquitos locale. On the whole, our forecasts are poorer here despite wider error-bars, in relative terms (incidence is overall lower), with both phenomena arising due to the much smaller amount of historical data. Recall that data are only available for five seasons before the first forecasting season, 2005/2006. The *right* panel of Figure A2 of Appendix A.2 shows that at least three of these eight forecasting seasons represented extrapolations, as there are no “nearby” historical seasons to match on. (And this fact is of course not known to the predictor at the start of the season.) For example, seasons 2007/2008, 2008/09 and 2010/2011 (corresponding to labels 3, 4, and 6 in Figure A2) are particularly “isolated”. These three also happen to have higher peak incidences than all but one of the previously observed seasons. As a result our early season forecasts of peak incidence well undershoot and undercover. However, as we show below, these predictions (and their corresponding log scores) compare favorably to the other contest entrants. All entrants found these seasons particularly hard to predict.

5.2 Relative view

Our summary of the contest results is more inclusive than the absolute results above. We are careful to delineate between our original, somewhat rushed, hybrid GLM/GP entry, and our newer, separate results for the revamped `hetGP` and the pure GLM-based predictor, although those were not actually entered into the contest. The main contest evaluation metric was log score, with larger being better, and contest winners were determined by aggregate scores reported for roughly the first half of the season. Contest organizers provided us with the full suite of aggregate four-weekly scores for all entrants, and it is these results that we display, and compare here. Unfortunately, these scores have been anonymized; we do not know who participated in the development of the methods, nor the details of how the methods were comprised, with the exception of a “baseline” SARIMA $(1, 0, 0)(4, 1, 0)_{52}$ model developed by the contest organizers.

Figure 7 shows log scores for the three targets on the San Juan data. Some of our comparator’s lines in the plots, including the “baseline”, are cut off because their log scores contained `NaN` or `-Inf` values. Observe that our team, via the the original hybrid GP/GLM submission (red), the GLM only (blue), or the new `hetGP` (green) has among the top average log scores for all three targets with the exception of a handful of weeks for total season incidence (right panel). Our best results are for the new `hetGP` comparator on the peak week target (middle panel), being by far highest (on average) for the first thirty weeks of the

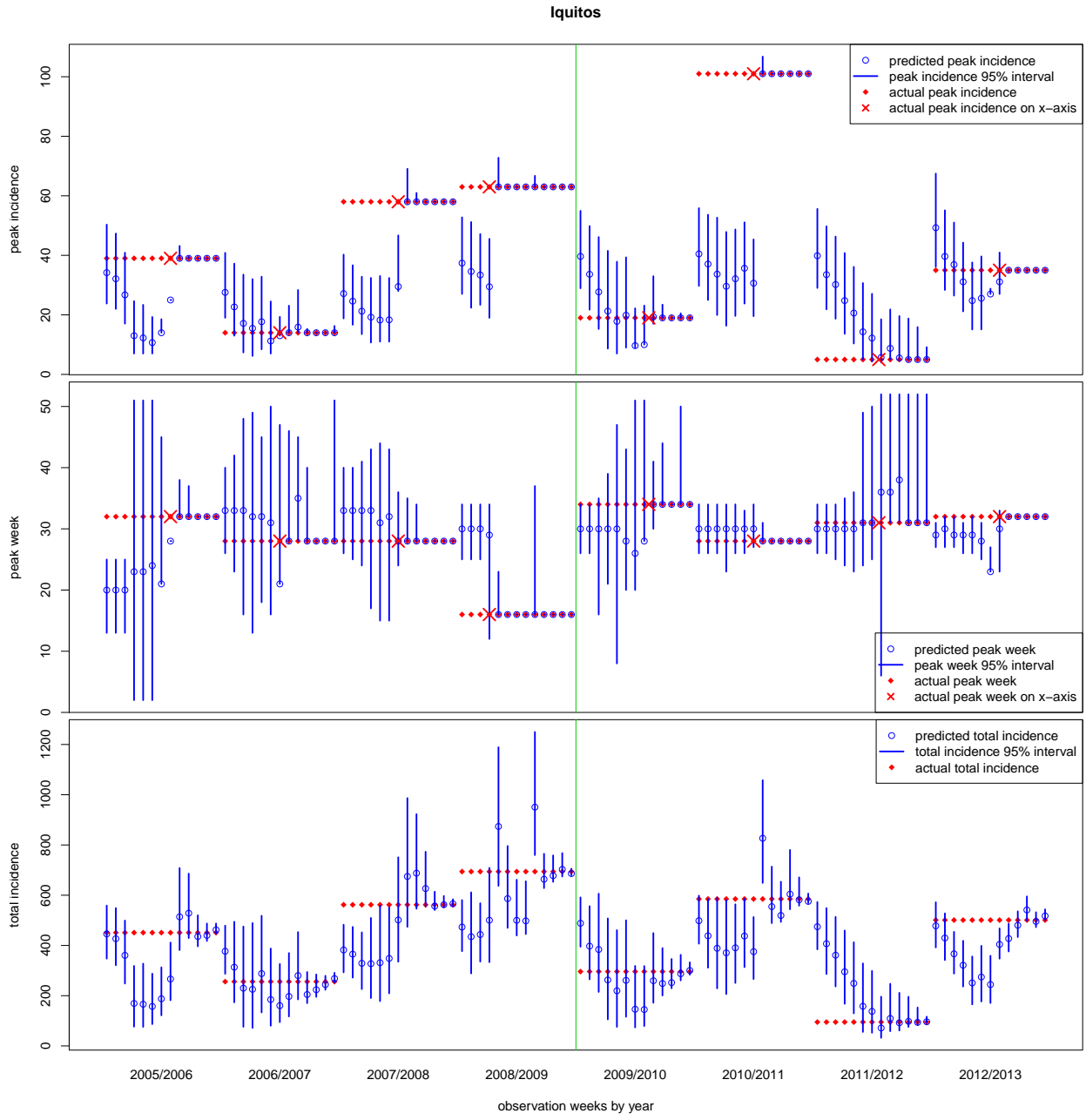


Figure 6: Weekly progress for Iquitos, mirroring the setup of Figure 5.

season, and competitive with the best thereafter. In the case of peak incidence our methods are in the top three for the first thirty weeks (and our GLM in blue leads for the first 8 weeks). Although our original hybrid outperforms the new `hetGP` comparator for the first thirty weeks, that order reverses for the latter twenty with `hetGP` giving the very best log scores for the peak incidence target.

Again the story is similar for Iquitos, with log scores from the contest being displayed in Figure 8. The scores are noisier due to the smaller amount of training data. Although our

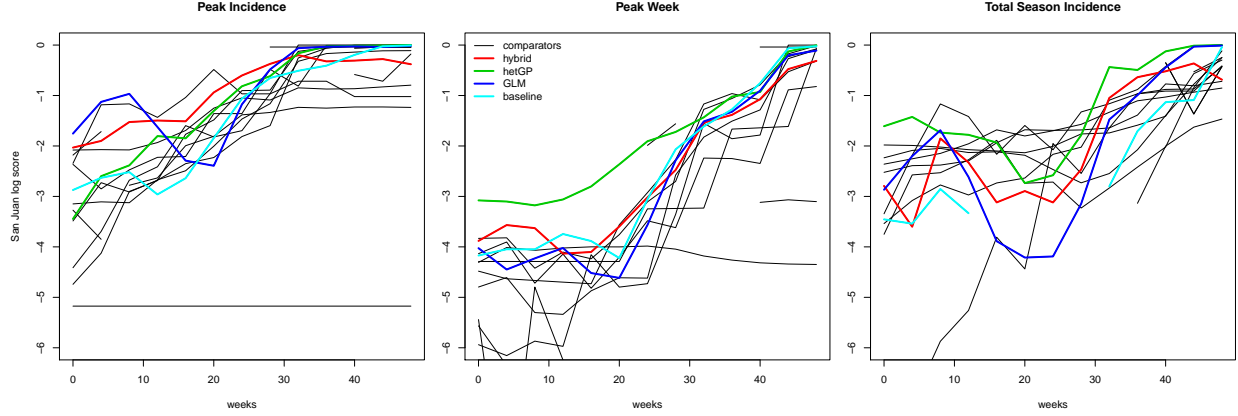


Figure 7: San Juan contest results via four-weekly average log score. Our original hybrid GP/GLM predictor is in red; our new `hetGP` in green, and the GLM in blue.

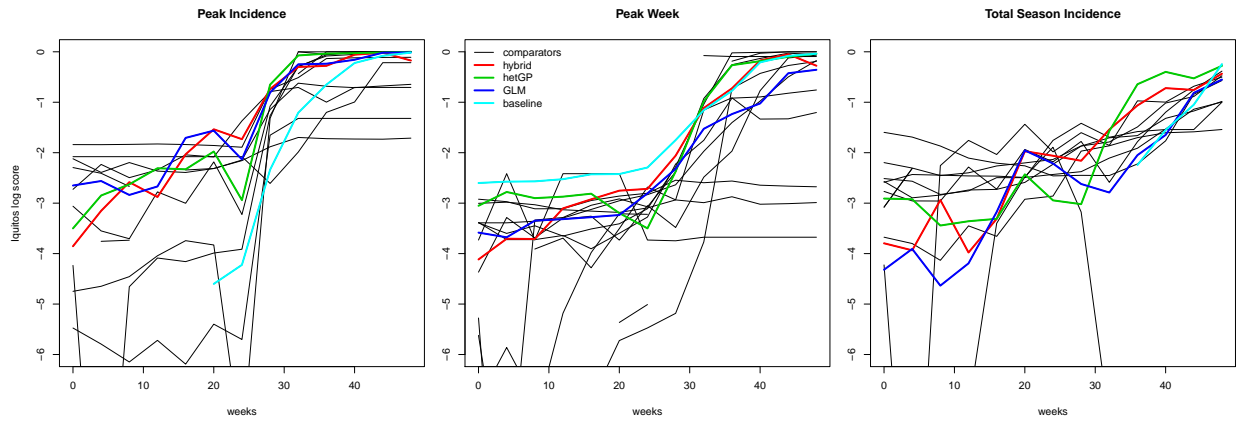


Figure 8: Iquitos contest results on the three targets.

comparators, new and old, are bested by some of the others in early weeks, those comparators which dominate early on are actually among some of the more inferior alternatives for latter weeks in the season. Observe that although the ‘‘baseline’’ gives excellent early peak week forecasts, for some reason it gives invalid values for the other targets during those weeks, a discussion we return to momentarily in more aggregate form.

Across both San Juan and Iquitos our methods tend to struggle early on to predict total season incidence, in both relative (Figures 7–8) and absolute (Figures 5–6) terms. To some degree this is by design. For the `hetGP` and the original hybrid GP/GLM, the initial severity indicator (x_4) may be overly pessimistic. Consequently, we tend to overestimate the number of cases we expect to see in low to moderate years. This seemed sensible as a conservative play, say in terms of human life: better to over-estimate incidence early on, and revise downwards if warranted. In unprecedented seasons (in the sense that such extreme dynamics were not previously observed), all of the comparators suffered. Our methods gained

a relative advantage through learning those “steep” dynamics somewhat more quickly, and recovering to nominal out-of-sample coverages faster compared to the others.

method	San Juan			method	Iquitos		
	Peak	Week	Season		Peak	Week	Season
A	4.92	3.81	5.85	A	4.81	2.27	7.23
B	10.15	13.54	³ 14.31	B	¹ 15.54	7.15	14.00
C	14.15	12.00	13.77	C	12.38	10.77	13.00
D	14.35	5.27	10.77	D	12.31	4.81	7.69
F	5.12	7.62	4.04	F	9.19	8.00	3.77
G	13.08	11.00	² 15.00	G	12.92	11.00	14.15
H	11.62	11.38	11.00	H	13.31	13.62	³ 14.46
I	2.85	4.54	3.15	I	8.88	8.15	3.77
J	12.00	11.31	14.15	J	12.08	9.77	13.15
K	8.46	7.15	5.12	K	3.19	7.69	3.77
L	5.62	3.81	3.15	L	3.19	5.08	3.77
M	5.69	3.81	6.31	M	7.23	9.92	10.23
N	4.92	11.08	13.00	N	5.77	11.85	² 15.85
O	12.85	³ 15.62	14.00	O	11.15	13.46	¹ 15.92
P	7.77	5.38	4.23	P	7.65	10.23	3.77
hybrid/E	³ 14.69	14.92	13.08	hybrid/E	13.92	³ 13.92	14.00
hetGP	¹ 15.23	¹ 18.08	¹ 17.31	hetGP	² 14.92	² 14.69	14.00
GLM	² 14.92	13.85	13.31	GLM	³ 14.31	10.92	11.00
baseline	11.62	² 15.85	8.46	baseline	7.23	¹ 16.69	6.46

Table 1: Average ranks of the log scores from Figures 7 (*left*) and 8 (*right*) over forecasting weeks. The alphabetic names A–P are the anonymized names from the CSV file provided by the CDC at the end of the contest period. Our hybrid GP/GLM was comparator “E” in that file. Higher ranks are better. Superscripts denote the top three in each column.

Table 1 provides a summary of lines in the figures above in terms of average ranks across *all* weeks for each comparator. A rank of one, the lowest value, is used for comparators with log scores of `NaN` or `-Inf`, a generous setting considering an infinitely poor score. Observe that our `hetGP` comparator makes a clean sweep on San Juan, having the highest average rank for each of three targets (*left table*). For Iquitos (*right table*), which is trained on far less historical data, the results are more scattered. Our `hetGP` comparator comes in second for both peak incidence and peek week. Comparators “B” and the “baseline”, which came in first in those two targets, respectively, happen also to be the bottom 40% of comparators on the alternate target. In other words, where one got the magnitude right, it was off in the timing, and vice versa. Our second place results would seem to offer some robustness here. On the final target, season incidence, our `hetGP` comparator was beaten out by four other teams, however observe that success on this target is bimodal, with very few ranks between 4 and 12. In total, our `hetGP` comparator was in the top two for five of the six targets, and was the only method to obtain an average rank of 14 or higher across all six targets.

6 Discussion

In 2015 several US governmental agencies jointly proposed a forecasting competition focused specifically on dengue, a vector borne disease endemic to tropical climates, to attract interest to the challenging and very important problem of learning to predict the observed patterns of disease occurrence and its relationship with its environment. Our team participated in the contest and our submission was chosen as one of six winners. In particular our hybrid GP/GLM forecasts were best overall for San Juan peak incidence. This hybrid submission was based more on pragmatics and a desire to hedge than it was on a belief that that hybridization was best suited to the problem at hand.

In this paper we presented an updated GP methodology. The biggest aspect of that revamp was the addition of explicit heteroskedastic errors that could vary with the severity of the season. This required new inference methodology and a bespoke implementation in code. A library called `hetGP` is soon to be released on CRAN. It compares favorably to the hybrid GP/GLM contest submission, although it does not uniformly dominate that method, which perhaps suggests that our hedge for the submission was a sensible one.

We note that a simpler alternative to our `hetGP` could involve separately fitting three independent GP predictors with data differentiated by the x_4 (severity) coordinate. However, one downside would be much less data for each GP fit, and once the data is partitioned by x_4 , that variable could no longer serve its dual role of encouraging nonstationary mean diversity in the spirit of Bornn et al. (2012), as described in Section 3.2. Our single GP, linking mean and nugget via x_4 , offers a parsimonious compromise between signal and noise modeling.

Our more conventional GLM alternative relied heavily on historical environmental and case data. Its forecast accuracy depends crucially on accurate sub-modeling of environmental components. Our sub-modeling approach was based on simple linear models. Using richer climate based sub-models models would almost certainly improve forecasts of the predictors and so improve predictions of incidence. However, quantifying the uncertainty in the GLM would still require significant Monte Carlo simulation. Further, climate models come with their own, sometimes daunting, computational demands. The added complexity and assumptions thus needed to improve the GLM approach adds support to a “simpler” phenomenological GP approach.

Although it is by no means perfect, it is surprising how well a phenomenological non-parametric, nonlinear predictor can do with no other data than the time series of values themselves (and stylized facts gleaned from a simple visual observation of that series of values). There is clear potential for improvement, and one possible avenue may be to interject more covariate information into the GP framework, in a similar way as in the GLM. However, as with the GLM, more historical data means more to forecast forward. When such covariates are unavailable or untrustworthy, as might arise with a newly emerging/establishing disease in a part of the world without reliable instrumentation and demographic surveys, an ability to construct reliable forecasts solely from observed counts of the number of confirmed cases may prove handy indeed.

Predictions from phenomenological models have the potential to inform mechanistic modeling efforts. For example, our GLM or `hetGP` could serve as a baseline against which mecha-

nistic models can be tested. Or, `hetGP`-based forecasts could be fed into mechanistic models of interventions and their costs, as entertained in the setups of Merl et al. (2009); Ludkovski and Niemi (2010) and Hu and Ludkovski (2015). All three of those papers involve forward simulations that use SIR-type models to evolve dynamics and thus to calculate potential costs and benefits of interventions. It has previously been noted that uncertainty in parameter values and in model structure for SIR-type models can result poor prediction and in sub-optimal and more costly interventions (Elderd et al., 2006). Our methods make no such mechanistic modeling assumptions and may provide more robust predictions of cases.

Although our `hetGP` approach needs much less data than the GLM approach (a few seasons of cases vs. 5-10 seasons of cases plus environmental data) it is still very much tuned to learning about patterns of a particular disease for a particular location. Thus, we expect it will be much more useful for predicting cases and planning responses for seasonal outbreaks of established infectious diseases in specific locations as opposed to outbreaks of novel, emerging epidemics. An exception may be for new vector-borne diseases that are transmitted by the same vector as the focal infection, for example Zika which is transmitted by the same mosquitoes as dengue. This could be an area for future exploration.

Acknowledgments

LRJ, EM, JR, SJR, and AMS acknowledge partial support from National Science Foundation (NSF) grant DEB-1518681. RBG acknowledges partial support from NSF grant DMS-1521702. EM acknowledges funding from: NSF grant DEB-1640780; the Stanford Center for Innovation in Global Health – Seed Grant Program; and the Stanford Woods Institute for the Environment – Environmental Ventures Program. JR acknowledges partial support from NSF grant EF-1241889, the National Institutes of Health grants R01GM109499 and R01TW010286-01. We gratefully acknowledge the agencies sponsoring the dengue forecasting challenge for collating and sharing the dengue incidence and environmental covariate data, and for producing and supplying the anonymized challenge metrics.

A Data properties

A.1 Variance stabilizing transformations

The original data are positive counts of the number of infected individuals in each week, which we have been calling the weekly incidence. As typical in such setups, there is a mean–variance relationship, with variance increasing as the mean increases. When modeling such data with Gaussian errors, as we describe in Section 3, it helps to deploy a variance stabilizing transformation. Figure A1 shows two such common transformations, based on the logarithm and the square root (bottom two panes; with the original series at the top). Observe that the log transformation does a good job of stabilizing the largest variances (occurring with the largest means), but over-expands the disturbances in values corresponding to the smallest means. The square root transformation (bottom) offers better balance.

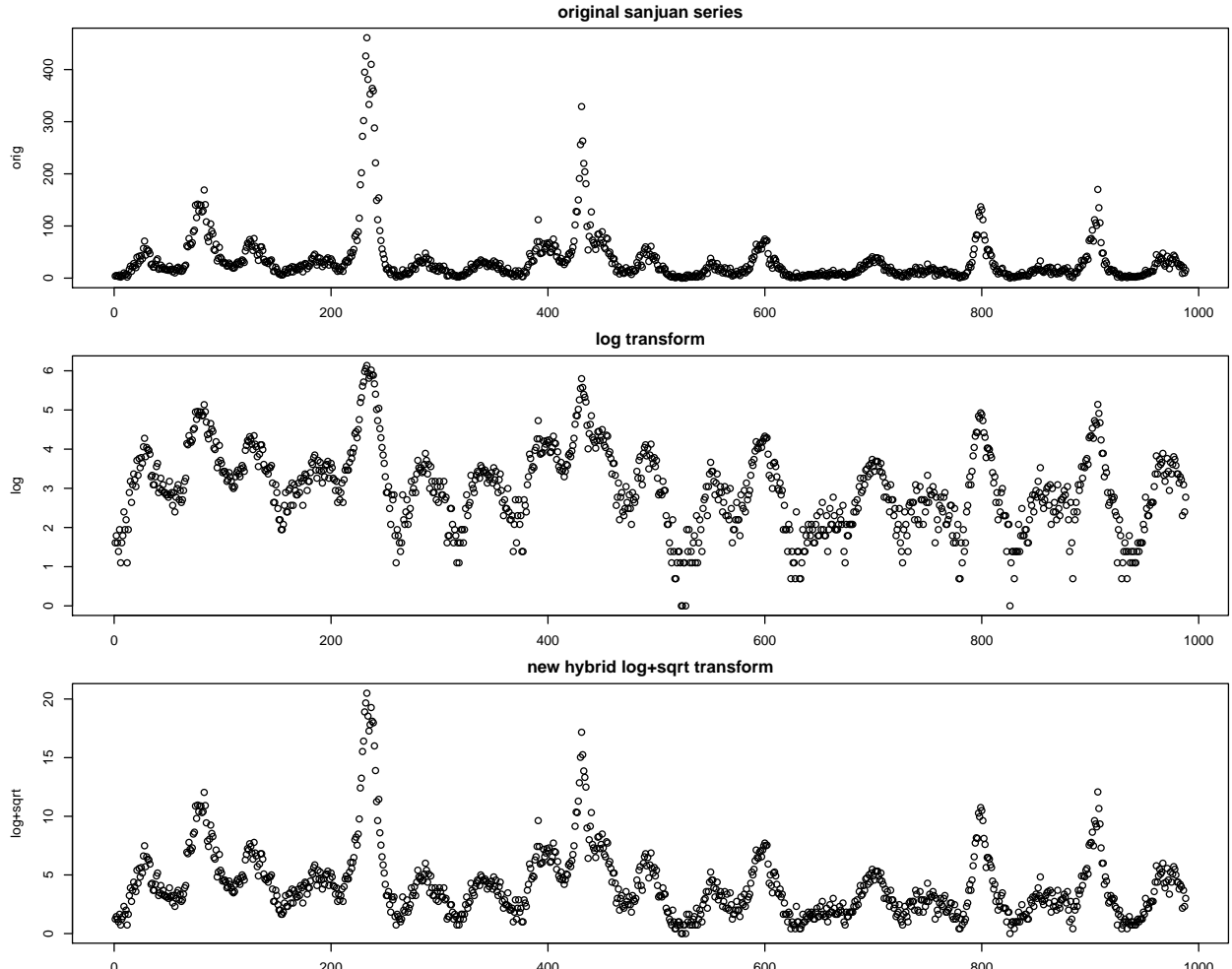


Figure A1: Original San Jan data over the first 1000 weeks (top panel); a log transformed version (middle); and a square root (bottom).

Our original contest submission used the log. The revised version we prefer in this paper is based on the square root, modified to account for the possibility that Gaussian forecasts on the transformed scale could be negative. In that case, the axis symmetry offered by inverting with a square is inappropriate. We therefore prefer the following forward/inverse pair:

$$f(x) = \begin{cases} \sqrt{x+1} - 1 & x \geq 0 \\ \log(x+1) & -1 < x < 0 \end{cases} \quad f^{-1}(y) = \begin{cases} (y+1)^2 - 1 & y \geq 0 \\ \exp(y) - 1 & \text{otherwise.} \end{cases}$$

Since the actual data contain no negative values, the log term in $f(\cdot)$ is never actually used. I.e., the “forward” transformation is a square root. However, the \exp in the f^{-1} is indeed relevant for converting Gaussian forecasts back to the original scale. It is especially so when evaluating the distribution of the forecasting targets [Section 2.2] via Monte Carlo [Section 4.2]. The ± 1 terms above ensure that the transition between square root and log segments, and their square and exponential inverses is continuous.

A.2 True targets

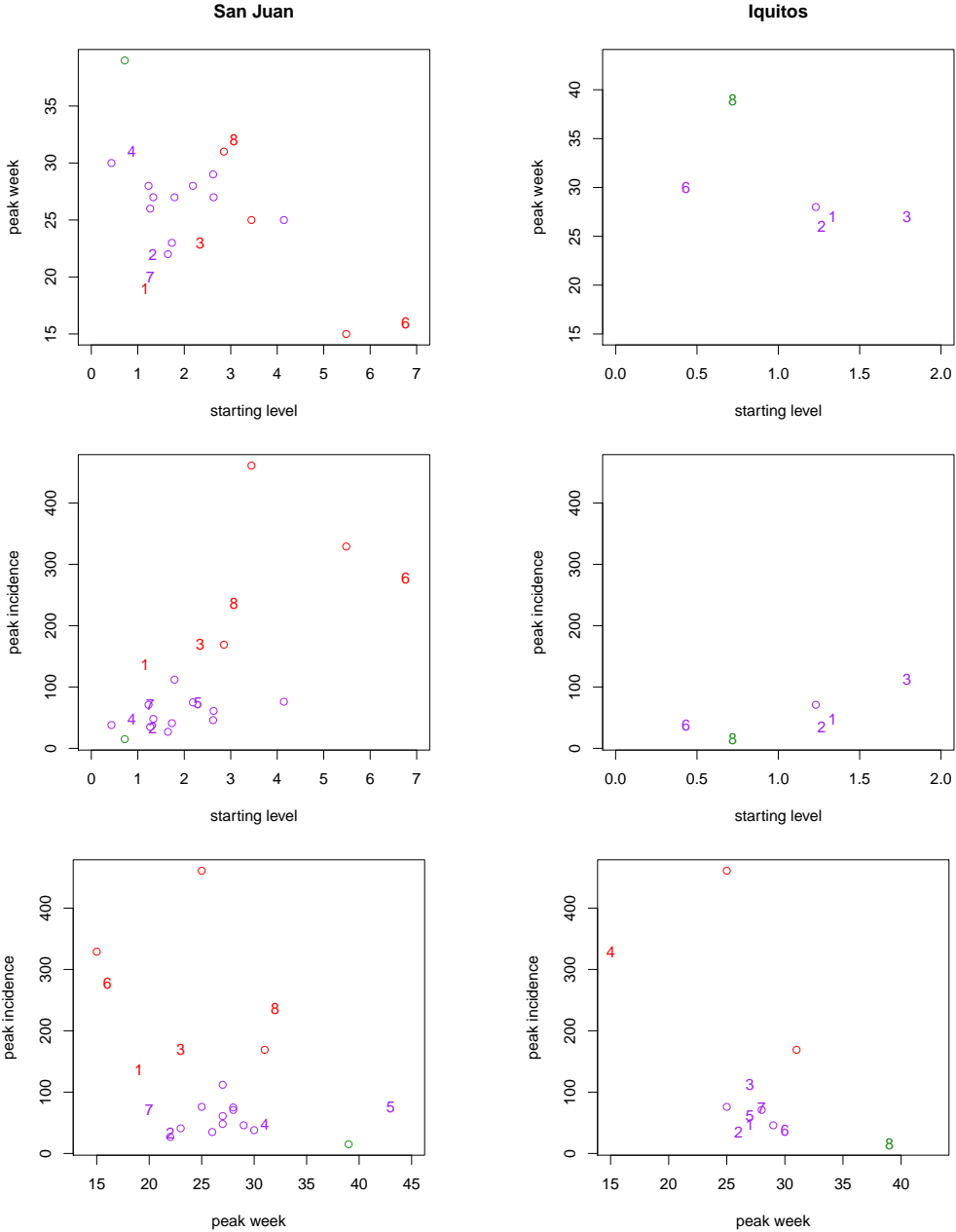


Figure A2: True target levels and starting locations for each season. The historical, i.e., those not shown in Figures 5–6, are open circles. The numbered points correspond to the seasons in those figures from left to right. Colors indicate the true severity labeling.

To get a sense of the difficulty of forecasting the dynamics of some of the seasons, especially for Iquitos which has many fewer historical seasons for training, Figure A2, shows a view into the peak incidence and peak week targets plotted against the starting level in each

season, as well as against themselves. The historical data, i.e., corresponding to the plot in Figure A1 for San Juan, which does not overlap with the forecasting seasons summarized in 5–6, are plotted as open circles. The numbered points correspond to the season, from left to right, shown in those figures. Observe that for San Juan, the numbered forecasting seasons are close to the historical seasons, making the prediction problem rather easier. An exception may be season 8, corresponding to 2012/13, as discussed in the Section 5.1. For Iquitos, those numbered forecasting seasons are rather farther from the historical seasons, indicating a much harder prediction problem. Indeed many of these forecasting seasons require extrapolations from the historical data. An exception may be season 7, corresponding to 2011/2012, which benefits from an earlier forecasting season (2: 2006/07) being nearby.

B Heteroskedastic MLE GP inference

The log likelihood for a zero-mean GP with covariance $\tau^2(C_n + \Lambda_n)$ is

$$\ell(\tau^2, \theta, \eta) \equiv \log L(\theta, \eta) = c - \frac{n}{2} \log \tau^2 - \frac{1}{2} \log |C_n + \Lambda_n| - \frac{Y_n^\top (C_n + \Lambda_n)^{-1} Y_n}{2\tau^2} \quad (6)$$

where η are the free parameters in Λ_n , e.g., a scalar nugget η in the typical homoskedastic version $\Lambda_n = \eta \mathbb{I}_n$ outlined in Section 3.1; or $(\eta_{-1}, \eta_0, \eta_{+1})$ defining $\lambda_1, \dots, \lambda_n$ in the heteroskedastic generalization of Section 3.3. An MLE for τ^2 may be derived as.

$$\begin{aligned} \frac{\partial \ell}{\partial \tau^2} &= -\frac{n}{2\tau^2} + \frac{Y_n^\top (C_n + \Lambda_n)^{-1} Y_n}{2(\tau^2)^2} \\ \hat{\tau}^2 &= \frac{Y_n^\top (C_n + \Lambda_n)^{-1} Y_n}{n}. \end{aligned} \quad (7)$$

Plugging $\hat{\tau}^2$ into (6) yields the so-called *concentrated* log likelihood

$$\hat{\ell}(\theta, \eta) = c - \frac{n}{2} \log Y_n^\top (C_n + \Lambda_n)^{-1} Y_n - \frac{1}{2} \log |C_n + \Lambda_n|. \quad (8)$$

Obtaining MLE's for the remaining (vectorized) parameters (θ, η) requires numerical techniques benefiting from a closed form gradient expression for the concentrated log likelihood (8). Two useful matrix derivative results are

$$\begin{aligned} \frac{\partial \Sigma^{-1}}{\partial \cdot} &= -\Sigma^{-1} \frac{\partial \Sigma}{\partial \cdot} \Sigma^{-1} \\ \frac{\partial \log |\Sigma|}{\partial \cdot} &= \frac{1}{|\Sigma|} \frac{\partial |\Sigma|}{\partial \cdot} = \frac{|\Sigma| \text{tr} \left\{ \Sigma^{-1} \frac{\partial \Sigma}{\partial \cdot} \right\}}{|\Sigma|} = \text{tr} \left\{ \Sigma^{-1} \frac{\partial \Sigma}{\partial \cdot} \right\}. \end{aligned}$$

Here $\frac{\partial \Sigma}{\partial \cdot}$ indicates a matrix comprised of entry-wise partial derivative calculations on Σ_{ij} .

Let $\dot{C}_n^{(k)} = \left\{ \frac{\partial C_{\theta}}{\partial \theta_k} \right\}_{ij}$ denote the matrix of derivatives of the correlation structure with respect to θ_k . In the case of our preferred separable Gaussian kernel (1) we have

$$\dot{C}_n^{(k)} = C_n \left\{ \frac{(x_{ik} - x_{jk})^2}{\theta_j^2} \right\}_{ij}.$$

Since Λ_n depends on η and not θ we have $\frac{\partial}{\partial \theta}(C_n + \Lambda_n) = \frac{\partial}{\partial \theta}C_n$. Therefore,

$$\frac{\partial \hat{\ell}}{\partial \theta_k} = \frac{n}{2} \times \frac{Y_n^\top (C_n + \Lambda_n)^{-1} \dot{C}_n^{(k)} (C_n + \Lambda_n)^{-1} Y_n}{Y_n^\top (C_n + \Lambda_n)^{-1} Y_n} - \frac{1}{2} \text{tr} \left\{ (C_n + \Lambda_n)^{-1} \dot{C}_n^{(k)} \right\}. \quad (9)$$

In the case of the nugget, vectorized or otherwise, $\frac{\partial}{\partial \eta}(C_n + \Lambda_n) = \frac{\partial}{\partial \eta}\Lambda_n$ because C_n does not depend on η . In the case of scalar η , $\frac{\partial}{\partial \eta}\Lambda_n$ is the $n \times n$ identity matrix. Then we obtain

$$\frac{\partial \hat{\ell}}{\partial \eta} = \frac{n}{2} \times \frac{Y_n^\top (C_n + \Lambda_n)^{-1} Y_n}{Y_n^\top Y_n} - \frac{1}{2} \text{tr} \left\{ (C_n + \Lambda_n)^{-1} \right\}. \quad (10)$$

For a vectorized η , such as the three vector $\{\eta_{-1}, \eta_0, \eta_{+1}\}$ determined by x_{i4} , $i = 1, \dots, n$, observe that $\dot{\Lambda}_n^{(k)} = \frac{\partial \Lambda_n}{\partial \eta_k}$ is a zero matrix with the exception of ones in positions i where $x_{i4} = k$ for $k \in \{-1, 0, +1\}$. This yields an expression for the partial derivative of the log likelihood that resembles (9), except for η_k

$$\frac{\partial \hat{\ell}}{\partial \eta_k} = \frac{n}{2} \times \frac{Y_n^\top (C_n + \Lambda_n)^{-1} \dot{\Lambda}_n^{(k)} (C_n + \Lambda_n)^{-1} Y_n}{Y_n^\top (C_n + \Lambda_n)^{-1} Y_n} - \frac{1}{2} \text{tr} \left\{ (C_n + \Lambda_n)^{-1} \dot{\Lambda}_n^{(k)} \right\}. \quad (11)$$

However, since each Λ_k is mostly zero it can be more efficient to perform calculations following the homogeneous derivative (10) on the n_k -sized subset of the data agreeing with $x_{i4} = k$.

In our supplementary material we provide a C implementation of likelihood and gradient for both homoskedastic and heteroskedastic versions together with an optimization wrapper that utilizes R's C back-end for the `method="l-bfgs-b"` to the built-in `optim` function. Prediction wrapper functions in R accessing underlying C implementations of Eq. (3) are also included. Examples are provided on the dengue contest data, together with optimization of latent x_{i4} settings, as well as stand-alone examples on other toy data.

C GLM details

Below we summarize some of the implementation details of our GLM-based scheme, outlined in Section 4.1. We first discuss the universe of variables searched via `step` and BIC; then basic reproductive rate R_0 predictor; and finally present out-of-sample forecasting results in a similar spirit to those provided in Section 5.1 for GP-based forecasts.

C.1 GLM universe of predictors

Tables 2 provides a summary of the covariates entertained as a universe of potential predictors for San Juan and Iquitos dengue incidence, respectively. Separate entries are provided for each transformation, with lags indicated, and the tables are separated in smoothed (via a one-sided 10-week `filter`) and un-smoothed (“raw”) categories, with the latter including the deterministic predictors. These universes define the `scope` provided to our automated

	SJ	Iq	name	lags	description
Raw	✓	✓	t	-	time since the first modeled response
	✓	✓	ci	-	cumulative observed cases in <i>previous</i> 52 weeks
	✓	✓	sin + cos	-	(both included) with periods of 52 and 26 weeks
Smooth	✓	✓	ly	1	log cases observed (i.e., an AR(1) term)
	✓	✓	lgm	-	average of current week's log cases over all <i>previous</i> seasons
	✓		lpop	1	log weekly population size
	✓	✓	lp	1	log precipitation
	✓	✓	lp ²	1	squared log precipitation
	✓	✓	tavg	1,11	average temperature
	✓	✓	tavg ²	1,11	squared average temperature
	✓		ndvi.45	1,16	value of NDVI at location [18.45, -66.14]
	✓		ndvi.50	1,11	value of NDVI at location [18.50, -66.14]
	✓		ndvi.avg	1	average of the four NDVI (raw climatology) values provided
	✓	✓	R_0	1,11	average value of scaled basic reproductive rate [Appendix C.2]
	✓		nino12	1,6,32	value of El Niño 1/2
	✓		nino12	1	value of El Niño 1/2
	✓		soi	1,24	Southern Oscillation Index
	✓		soi	1	Southern Oscillation Index

Table 2: Universe of variables entertained for San Juan (SJ) and Iquitos (Iq) stepwise search by. Lags are provided in weeks.

step-wise BIC selection via `step` in R. They were determined by an extensive exploratory analysis performed on the training data, separately for San Juan and Iquitos.

A few brief notes on Table 2 follow. The time predictor, t , is the index of the observation under study, included to capture a linear trend. Although sin and cos share an entry, both predictors (at both periods) are entertained, together comprising of four deterministic “covariates”. There were a small number of missing values in the NDVI series provided by the contest organizers. We performed a simple GP-based prediction to infill the missing values and ignored their uncertainty in our analysis. Our universe of variables was smaller for Iquitos due to the smaller amount of data, and overall lower degree of predictability, despite the smaller scale of incidence in most seasons. This is handled through a smaller number of lags (El Niño and SOI) and some averaging (NDVI) of the environmental covariates. Only yearly population figures were available for each location. Weekly populations were constructed for each site using simple linear interpolation.

As a reminder, we modeled the `total_cases` response with a negative binomial GLM using a log link. We also entertained a log-linear model (i.e., Poisson GLM), but a residual analysis revealed underestimated spread. The log-linear model also under-performed in a cross-validated prediction exercise on the training data (not shown).

C.2 Basic reproductive rate predictor

We deployed a derived predictor, scaled R_0 (i.e., basic reproductive rate) as a function of temperature. The basic reproductive rate is defined as the expected number of new cases of an infectious disease that will be caused by a single infected individual introduced into a

naive (entirely susceptible) population. If $R_0 > 1$ an epidemic is expected to occur whereas if $R_0 < 1$ the disease will not spread. It is used as a standard, convenient measure of how easily a disease is transmitted and how hard it is to control. For vector-borne disease, the value of R_0 depends on vector (here mosquito) traits such as mortality rates, biting rates, reproduction, etc. Full details of parameterized versions of R_0 from data are given by Mordecai et al. (2017). Here we present an abbreviated description as is relevant to dengue forecasting via GLMs.

Data were collected on the viruses and mosquito vital rates from assorted laboratory studies that observed *Aedes spp.* mosquitoes, a dengue vector, and dengue virus prevalence at a range of constant temperatures. Although raw data were preferred, if the experimenter was unreachable then data were collected by hand from tables or figures digitized using WebPlotDigitizer. Following the methods laid out by Mordecai et al. (2013) and Johnson et al. (2015) we calculated a Bayesian posterior for parameters involved in a functional thermal response for each trait. More specifically, we fit unimodal thermal responses for each temperature sensitive portion of the mosquito/pathogen system. These posteriors were then combined together to derive a distribution of R_0 :

$$R_0 = \sqrt{\frac{M}{Nr} \frac{a^2 bc \exp(-\mu/\text{PDR})}{\mu}}, \quad (12)$$

where M is the density of mosquitoes, a is the bite rate, bc is vector competence, μ is the mortality rate of adult mosquitoes, PDR is the parasite development rate (1/EIP, the extrinsic incubation period of the parasite), N is the human density, and r is the human recovery rate. Following Mordecai et al. (2013), we take

$$M = \frac{\text{EFD} \cdot p_{\text{EA}} \cdot \text{MDR}}{\mu^2}, \quad (13)$$

where EFD is number of eggs produced per female per day, p_{EA} is the probability that an egg will hatch and the larvae will survive to the adult stage, and MDR is the mosquito development rate. All of the parameters that describe mosquito or parasite traits (i.e., everything except N and R) are assumed to depend on temperature.

R_0 is also influenced by factors other than temperature, and the particular value at any location depends on the number of susceptible humans at that location and socio-economic factors that impact whether humans and mosquitoes interact. We do not have access to data as part of this challenge to estimate these values, and anyways the GLM would naturally rescale this predictor. Thus, we used the posterior mean of $R_0(T)$ rescaled to lie between [0,1] as the predictor in our model.

References

Ankenman, B. E., Nelson, B. L., and Staum, J. (2010). “Stochastic kriging for simulation metamodeling.” *Operations Research*, 58, 371–382.

Barrera, R., Amador, M., and MacKay, A. J. (2011). “Population dynamics of *Aedes aegypti* and dengue as influenced by weather and human behavior in San Juan, Puerto Rico.” *PLoS Negl Trop Dis*, 5, 12, e1378.

Binois, M., Gramacy, R. B., and Ludkovski, M. (2016). “Practical heteroskedastic Gaussian process modeling for large simulation experiments.”

Bornn, L., Shaddick, G., and Zidek, J. (2012). “Modelling Nonstationary Processes Through Dimension Expansion.” *J. of the American Statistical Association*, 107, 497, 281–289.

Cressie, N. (1993). *Statistics For Spatial Data*, revised edition. John Wiley & Sons.

Degallier, N., Favier, C., Menkes, C., Lengaigne, M., Ramalho, W. M., Souza, R., Servain, J., and Boulanger, J.-P. (2010). “Toward an early warning system for dengue prevention: modeling climate impact on dengue transmission.” *Climatic Change*, 98, 3-4, 581–592.

Elderd, B. D., Dukic, V. M., and Dwyer, G. (2006). “Uncertainty in predictions of disease spread and public health responses to bioterrorism and emerging diseases.” *Proceedings of the National Academy of Sciences*, 103, 42, 15693–15697.

Farah, M., Birrell, P., Conti, S., and Angelis, D. D. (2014). “Bayesian Emulation and Calibration of a Dynamic Epidemic Model for A/H1N1 Influenza.” *Journal of the American Statistical Association*, 109, 508, 1398–1411.

Gagnon, A. S., Bush, A. B., and Smoyer-Tomic, K. E. (2001). “Dengue epidemics and the El Niño southern oscillation.” *Climate Research*, 19, 1, 35–43.

Gneiting, T. and Raftery, A. E. (2007). “Strictly proper scoring rules, prediction, and estimation.” *Journal of the American Statistical Association*, 102, 477, 359–378.

Gramacy, R. B. (2014). *laGP: Local Approximate Gaussian Process Regression*. R package version 1.1-4.

— (2016). “laGP: Large-Scale Spatial Modeling via Local Approximate Gaussian Processes in R.” *Journal of Statistical Software*, 72, 1, 1–46.

Hu, R. and Ludkovski, M. (2015). “Sequential design for ranking response surfaces.” *arXiv preprint arXiv:1509.00980*.

Johansson, M. A., Cummings, D. A., and Glass, G. E. (2009). “Multiyear climate variability and dengue—El Niño southern oscillation, weather, and dengue incidence in Puerto Rico, Mexico, and Thailand: a longitudinal data analysis.” *PLoS Med*, 6, 11, e1000168.

Johnson, L. R., Ben-Horin, T., Lafferty, K. D., McNally, A., Mordecai, E., Paaijmans, K. P., Pawar, S., and Ryan, S. J. (2015). “Understanding uncertainty in temperature effects on vector-borne disease: A Bayesian approach.” *Ecology*, 96, 203–213.

Kuhn, K., Campbell-Lendrum, D., Haines, A., Cox, J., Corvalán, C., Anker, M., et al. (2005). "Using climate to predict infectious disease epidemics." *Geneva: WHO*.

Lambrechts, L., Paaijmans, K. P., Fansiri, T., Carrington, L. B., Kramer, L. D., Thomas, M. B., and Scott, T. W. (2011). "Impact of daily temperature fluctuations on dengue virus transmission by *Aedes aegypti*." *Proceedings of the National Academy of Sciences*, 108, 18, 7460–7465.

Ludkovski, M. and Niemi, J. (2010). "Optimal dynamic policies for influenza management." *Statistical Communications in Infectious Diseases*, 2, 1, article 5.

Matheron, G. (1963). "Principles of Geostatistics." *Economic Geology*, 58, 1246–1266.

Merl, D., Johnson, L. R., Gramacy, R. B., and Mangel, M. (2009). "A statistical framework for the adaptive management of epidemiological interventions." *PloS One*, 4, 6, e5807.

Moore, C. G., Cline, B. L., Ruiz-Tibén, E., Lee, D., Romney-Joseph, H., and Rivera-Correa, E. (1978). "Aedes aegypti in Puerto Rico: environmental determinants of larval abundance and relation to dengue virus transmission." *The American Journal of Tropical Medicine and Hygiene*, 27, 6, 1225–1231.

Mordecai, E., Cohen, J., Evans, M. V., Gudapati, P., Johnson, L. R., Lippi, C. A., Miazgowicz, K., Murdock, C. C., Rohr, J. R., Ryan, S. J., Savage, V., Shocket, M., Stewart Ibarra, A., Thomas, M. B., and Weikel, D. P. (2017). "Detecting the impact of temperature on transmission of Zika, dengue and chikungunya using mechanistic models." *PLoS Negl Trop Dis*, 11, 4, e0005568.

Mordecai, E. A., Paaijmans, K. P., Johnson, L. R., Balzer, C., Ben-Horin, T., de Moor, E., McNally, A., Pawar, S., Ryan, S. J., Smith, T. C., and Lafferty, K. D. (2013). "Optimal temperature for malaria transmission is dramatically lower than previously predicted." *Ecology Letters*, 16, 1, 22–30.

R Development Core Team (2008). *R: A Language and Environment for Statistical Computing*. R Foundation for Statistical Computing, Vienna, Austria. ISBN 3-900051-07-0.

Rasmussen, C. E. and Williams, C. K. I. (2006). *Gaussian Processes For Machine Learning*. The MIT Press.

Reynolds, R. W., Rayner, N. A., Smith, T. M., Stokes, D. C., and Wang, W. (2002). "An improved in situ and satellite SST analysis for climate." *Journal of climate*, 15, 13, 1609–1625.

Stewart-Ibarra, A. M. and Lowe, R. (2013). "Climate and non-climate drivers of dengue epidemics in southern coastal Ecuador." *The American journal of tropical medicine and hygiene*, 88, 5, 971–981.

Stewart-Ibarra, A. M., Ryan, S. J., Beltrán, E., Mejía, R., Silva, M., and Muñoz, Á. (2013). “Dengue vector dynamics (*Aedes aegypti*) influenced by climate and social factors in Ecuador: implications for targeted control.” *PLoS one*, 8, 11, e78263.

Thomson, M. C., Garcia-Herrera, R., and Beniston, M. (2008). *Seasonal Forecasts, Climatic Change and Human Health*. Springer.

Venables, W. N. and Ripley, B. D. (2002). *Modern Applied Statistics with S*. 4th ed. New York: Springer. ISBN 0-387-95457-0.

World Health Organization (2009). *Dengue: guidelines for diagnosis, treatment, prevention and control*. World Health Organization: Special Programme for Research and Training in Tropical Diseases, Department of Control of Neglected Tropical Diseases, and Epidemic and Pandemic Alert.

— (2016). “Dengue vaccine: WHO position paper - July 2016.” *Weekly epidemiological record*, 91, 30, 349–364.

Xu, L., Stige, L. C., Chan, K.-S., Zhou, J., Yang, J., Sang, S., Wang, M., Yang, Z., Yan, Z., Jiang, T., et al. (2016). “Climate variation drives dengue dynamics.” *Proceedings of the National Academy of Sciences*, 201618558.